RSC Advances

PAPER

View Article Online
View Journal | View Issue

Cite this: *RSC Adv.*, 2014, **4**, 2267

Nanostructured palladium-reduced graphene oxide platform for high sensitive, label free detection of a cancer biomarker†

Vinod Kumar,[a] Saurabh Srivastava,[bd] Sima Umrao,[b] Ram Kumar,[b] Gopal Nath,[c] Gajjala Sumana,[d] Preeti S. Saxena*[a] and Anchal Srivastava*[b]

Received 22nd April 2013
Accepted 14th October 2013

DOI: 10.1039/c3ra41986j

www.rsc.org/advances

We report the results of studies related to the fabrication of a palladium nanoparticle decorated-reduced graphene oxide (Pd@rGO) based electrochemical immunosensor for the label free ultrasensitive detection of the prostate-specific antigen (PSA), a prostate cancer biomarker. The synergistic electrochemical activities of Pd and rGO result in an enhanced electron transfer used for the development of an ultrasensitive immunosensor. A facile approach was developed for the *in situ* synthesis of Pd@rGO using ascorbic acid as the reducing agent which enables the simultaneous reduction of both Pd^{+2} and GO into Pd nanoparticles and rGO, respectively. XRD, FTIR, SEM and TEM investigations were carried out to characterize the Pd@rGO material. A thin film of nanostructured Pd@rGO was electrophoretically deposited on an ITO coated glass electrode that was subsequently functionalized with anti-PSA antibodies. The electrochemical sensing results of the proposed immunosensor showed a high sensitivity {28.96 μA ml ng^{-1} cm^{-2}}. The immunosensor is able to detect PSA at concentrations as low as 10 pg ml^{-1}. The simple fabrication method, high sensitivity, good reproducibility and long term stability with acceptable accuracy in human serum samples are the main advantages of this immunosensor.

Introduction

Early and accurate diagnosis of cancer is a key challenge for the successful treatment of the disease. Among more than 200 types of human cancer, prostate cancer has become the second leading cause of cancer death in males. The prostate-specific antigen (PSA), a 33 kDa serine protease largely bound to endogenous protease inhibitors in serum, has been widely accepted as a biomarker of prostate cancer.[1–3] For healthy males, the PSA concentration level in serum ranges from 0 to 4 ng ml^{-1}. Routinely used diagnostic techniques based on morphological investigations such as magnetic resonance imaging (MRI) and ultra sonography (USG), have been used for the diagnosis of prostate related problems but have not been found to be sufficient for the detection of cancer. On the other hand, PSA tests measure total PSA levels *i.e.* the levels of free and bound PSA secreted by both normal and cancerous glandular cells of prostate,[4,5] which plays an important role towards the detection of cancer. Thus, proper monitoring of total PSA levels (other than through biopsy) is critical for the evaluation of the prostate cancer malignancy. Enzyme linked immunosorbent assays (ELISAs), fluorescence immunoassays,[6] chemiluminescent assays,[7] and time-resolved immunofluorometric assays[8,9] have been developed for PSA detection. ELISA is quite a promising technique but it is time consuming, requires labeling and is not sufficient for sensitive detection if the biomarker is present in very low concentrations (sub nanogram to picogram levels). However, methods other than ELISA, unfortunately, are either harmful to the health, time-consuming and labor-intensive, or require highly trained personnel and sophisticated instrumentation. Therefore, there is a strong need to develop a real-time, high sensitive, and label free sensing devices which may overcome the drawbacks of ELISA and the other methods.[10,11] In recent years, electrochemical biosensors have gained much interest due to their rapidity, high sensitivity and high signal to noise ratio as well as their relative inexpensiveness and low reagent consumption. In addition, electrochemical detection systems can be easily miniaturized without reducing their analytical performance.

[a]*Department of Zoology, Banaras Hindu University, Varanasi-221005, India. E-mail: pssaxena@rediffmail.com; mail2vinod2@gmail.com; Fax: +91 542-2368174; Tel: +91 542-2307149 ext. 109*

[b]*Department of Physics, Banaras Hindu University, Varanasi-221005, India. E-mail: saurabhnpl@gmail.com; anchalbhu@gmail.com; ramasharamyadav@gmail.com; Simaphy@gmail.com; Fax: +91 0542-2368174; Tel: +91 542-2307308*

[c]*Department of Microbiology, Institute of Medical Sciences, Banaras Hindu University, Varanasi-221005, India. E-mail: gopalnath@gmail.com*

[d]*Department of Science and Technology Center on Biomolecular Electronics, Biomedical Instrumentation Section, CSIR-National Physical Laboratory, Dr K.S. Krishnan Road, New Delhi-110012, India. E-mail: sumanagajjala@gmail.com*

† Electronic supplementary information (ESI) available. See DOI: 10.1039/c3ra41986j

Thus, electrochemical detection has emerged as a powerful technique for the rapid and sensitive detection of biomarkers even at low concentrations.[12]

Metal nanoparticles of palladium (Pd) and platinum (Pt), owing strong electrocatalytic properties, have shown tremendous potential in a wide range of applications, such as in energy storage, catalysis and in electrochemical sensors.[13–15] The electro-catalytic properties of these nanoparticles are largely influenced by the size and morphology of these materials. In this regard, a lot of work has been focused on improving the synthetic control over the size and morphology of these nanoparticles using different stabilizing agents.[16–18] Dispersing these nanoparticles on the surface of two dimensional nanomaterials (without stabilizers) might be a much better approach to access the excellent properties of these metal nanoparticles.

Graphene oxide (GO) and reduced graphene oxide (rGO) (derivatives of graphene) are 2-D nanostructures possessing a high surface area with strong chemical stability that have been used as a suitable matrix for the synthesis of various metal nanoparticles.[19] Because of their high surface area, GO and rGO provide the ideal support for the homogeneous dispersion of metal nanoparticles without affecting their electrochemical activities.[19]

Nanostructures of graphene with metal nanoparticles have expanded the range of applications due to their superior and even new functional properties *via* cooperative interactions. One of such examples is their application as electrode materials for the development of high performance biosensing devices, where the enhanced electron transfer leading to an efficient collection and transfer of electrons at the electrode surface may be anticipated.

In comparison to Pt nanoparticles, Pd nanoparticles have been a hot topic of interest due to their better catalytic activity and lower cost.[20–25] First principle calculations have also indicated the strong interaction and binding affinity of Pd nanoparticles and graphene.[26] Several methods have been reported for the synthesis of Pd nanoparticle decorated graphene sheets[27,28] using strong reducing agents. Two parameters of the nanostructure are crucial for their application towards the development of high sensitive biosensors: firstly, the electrical conductivity which is directly related to the signal amplification and secondly, the content in surface functionalities to achieve the loading of the maximum amount of biomolecules which leads to an enhanced sensitivity.

The current study is aimed to develop a single step facile method for the *in situ* synthesis of Pd@rGO with an improved conductivity while maintaining an enough surface functionality. Although GO possesses a larger number of oxygen functionalities than rGO, the reduced conductivity of GO in comparison to rGO restrict its further application as a sensitive platform for biosensing purposes. Therefore, a material in between GO and rGO is highly desirable as a high sensitive platform for biosensing purposes, which could be obtained by the controlled reduction of GO to rGO. Strong reducing agents (used in the earlier reported methods) do not meet such a requirement and this needs to be achieved by the use of a mild reducing agent. In the current study, ascorbic acid, a mild reductant, is used to achieve the controlled and simultaneous reduction of Pd^{+2} and GO to Pd^0 and rGO, respectively, in the same process, to finally obtain Pd@rGO while preserving the adequate functional groups (for bio-functionalization). The remained functional groups in Pd@rGO are not only important for bio-functionalization but play a crucial role towards the enhanced electron transfer. The synthesized Pd@rGO was further used for the development of a sensitive platform for the electrochemical detection of the PSA cancer biomarker.

Materials and methods

Materials

Graphite powder flakes (45 μm, >99.99 wt%), Na_2PdCl_4, L-ascorbic acid, prostate-specific antigen (PSA) and monoclonal anti-PSA antibody, bovine serum albumin (BSA), and human AB type serum (male) were purchased from Sigma-Aldrich Chemical Pvt. Limited, Bangalore, India. All other used chemicals were obtained from Merck India Pvt. Limited, Mumbai, India.

Synthesis of graphene oxide (GO)

Graphene oxide was synthesized using the improved Hummers method[29] with a slight modification. In brief, 0.0015 kg of graphite powder was pre-oxidized by reacting it with a mixture of 40 ml of 98% H_2SO_4, 5 g $K_2S_2O_8$ and 5 g of P_2O_5 for 4 h at 80 °C. The resulting suspension was washed with deionized water (DI) 4–5 times and vacuum dried at 50 °C. Further oxidation was achieved by adding the pre-oxidized graphite to a mixture of concentrated H_2SO_4–H_3PO_4 (v/v:180 : 13) with constant stirring. After 5 min, 9 g of $KMnO_4$ was added to the mixture and the stirring was continued for 15 h at 50 °C .The reaction was stopped after about 15 h and the reactants were allowed to cool at room temperature after which 200 ml of ice were poured into the mixture followed by 1.5 ml of H_2O_2 (30%). The fine material was separated from the mixture through a U.S. standard testing sieve of pore size 30 μm. The supernatant was discarded and the filtrate was subject to centrifugation at 5000 rpm for 3 h. Multiple washings of the sedimented material were carried out several times with DI water, 30% HCl and ethanol (100 ml of each) followed by centrifugation and separation. The final sediment was suspended in 100 ml of ether and filtered through a PTFE membrane with a pore size of 0.45 μm. The obtained semi-solid material was vacuum dried overnight to obtain brown graphene oxide (GO) powder.

In situ synthesis of the Pd@rGO nanostructure

5 ml (1 mg ml^{-1}) of an aqueous suspension of GO was mixed with 5 ml (10 mM) of an aqueous solution of Na_2PdCl_4 and stirred for 10 minutes at 50 °C. 1 ml (5 mM) of an aqueous solution of L-ascorbic acid was added drop by drop to the mixed suspension of GO and Na_2PdCl_4 followed by stirring for 2 h at 80 °C. 500 μl (1 mM) of KCl and KBr each were added during the reaction to prevent the agglomeration of the Pd nanoparticles. The product was collected by centrifugation and washed with DI water and dried. A schematic diagram related to the synthesis of Pd@rGO is shown in Fig. 1.

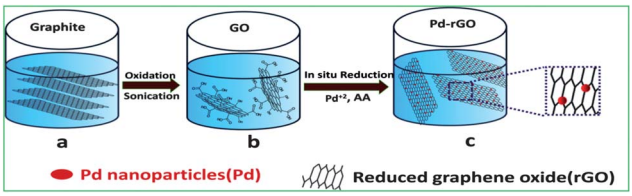

Fig. 1 Schematic representation of the synthesis of the Pd@rGO nanostructure.

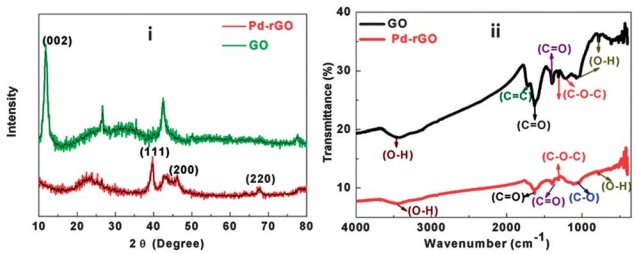

Fig. 2 (i) XRD pattern, and (ii) FTIR spectrum of GO and the Pd@rGO nanostructure.

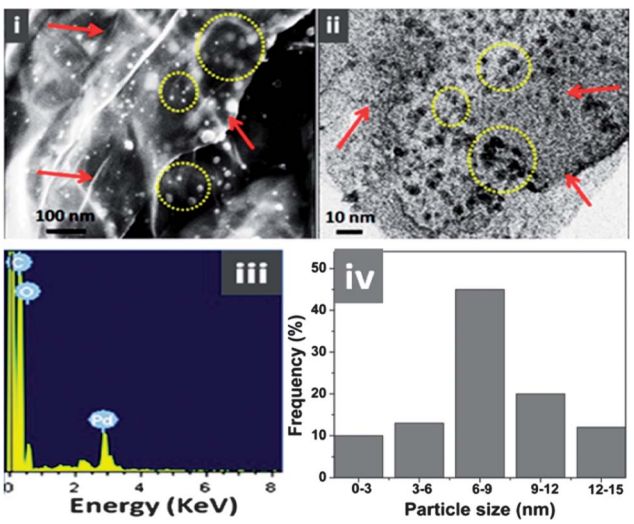

Fig. 3 (i) SEM micrograph and (ii) TEM micrograph of the Pd@rGO nanostructure, the red arrow shows the rGO nanosheets while the yellow circle indicate the presence of Pd nanoparticles, (iii) EDX of the Pd@rGO nanostructure and (iv) histogram showing the size distribution of the Pd nanoparticles (standard deviation, $\sigma = 14.47$).

Electrophoretic fabrication of the Pd@rGO/ITO electrode

A film of the Pd@rGO nanostructure was fabricated on a ITO coated glass substrate *via* the electrophoretic deposition (EPD) technique. A colloidal solution of the Pd@rGO composite (0.5 mg dl^{-1}) in acetonitrile was used for the EPD. Electrophoretic deposition was carried out using a two-electrode cell containing the colloidal suspension by applying a DC voltage (120 V) for 2 min. A platinum (Pt) foil (1 cm × 2 cm) acted as the cathode and a pre-cleaned ITO-coated glass substrate (sheet resistance of 30 Ω cm^{-1}) as the anode. The two electrodes separated by 1 cm were placed parallel to each other and dipped in the colloidal suspension of Pd@rGO in acetonitrile. In order to obtain a surface charge on the composite, 10^{-5} to 10^{-4} mol of $Mg(NO_3)_2 \cdot 6H_2O$ was added to the suspension as the electrolyte for EPD. The Mg^{2+} ions adsorbed on the nanostructure provide adequate positive surface charges to enable a uniform film deposition.[30] The deposited film was removed from the suspension and washed with DI water followed by drying.

Biofunctionalization of the Pd@rGO/ITO electrode surface with the anti-PSA antibody

Anti-PSA antibody was covalently attached to the surface of the Pd@rGO/ITO electrode through the formation of an amide bond between the $-NH_2$ groups of the antibodies and the –COOH groups of rGO on the surface of the Pd@rGO/ITO electrode. Prior to functionalization, the –COOH functional groups of the Pd@rGO/ITO electrode have been activated by well established EDC/NHS chemistry. 10 μg ml^{-1} of an anti-PSA antibody solution was freshly prepared in phosphate buffer (PBS, pH 7.4). 10 μl of the solution of the anti-PSA antibody was uniformly spread on the surface of the Pd@rGO/ITO electrode and was incubated overnight in a humid chamber. A bovine serum albumin (BSA) solution (1 mg ml^{-1}) was used to block the non-specific active sites present on the electrode surface. The BSA-anti-PSA/Pd@rGO/ITO immunoelectrode was washed with PBS and stored at 4 °C for further use.

Results and discussion

Characterization

The synthesized Pd@rGO nanocomposite was thoroughly characterized by X-ray diffraction (XRD, Rigaku), UV-Visible (Perkin-Elmer) and Raman spectroscopy (HR800 LabRam, Horiba/Jobin-Yvon). Structural and morphological characterizations were carried out using scanning electron microscopy (SEM LEO 440) and transmission electron microscopy (HRTEM, Tecnaii-G2F30 STWIN). Electrochemical studies were conducted using an Autolab potentiostat/galvanostat (Eco Chemie, The Netherlands).

XRD characterization

The crystalline structure of the Pd nanoparticles on partially reduced graphene oxide was identified by X-ray diffraction (XRD) (Fig. 2i). The intense peak at 11.4° corresponds to the (002) reflection plane and the peak at 42° corresponds to the (001) reflection plane of GO.[30] It is noteworthy that the diffraction peak at 26.4° corresponding to graphite is very weak, indicating the complete conversion of graphite into GO through the oxidative treatment (Fig. 2i). The Pd@rGO spectrum reveals diffraction peaks at 40°, 46.5° and 67.9° indexed to the (111), (200) and (220) crystalline planes of the faced centered cubic structure of the Pd nanoparticles, respectively (JCPDS no. 05-0681). The absence of the peak at 11.4° corresponding to the (002) reflection plane of GO in the Pd@rGO nanostructure indicates the conversion of GO to rGO during the synthesis. The

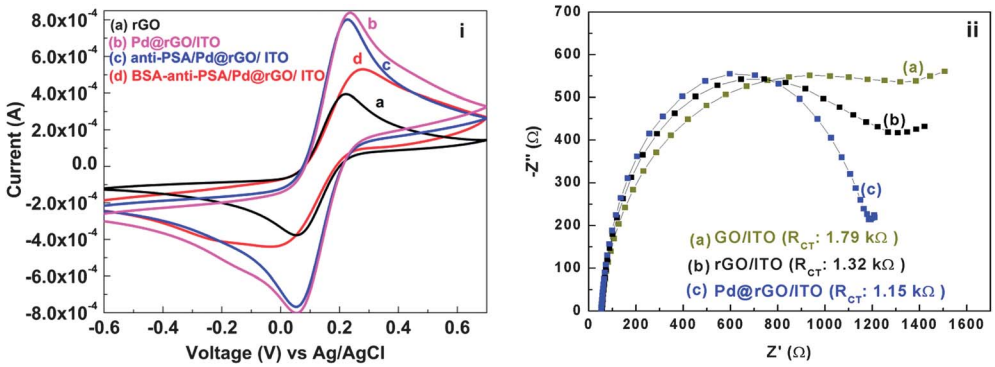

Fig. 4 (i) Electrochemical cyclic voltammograms (CV) of (a) rGO/ITO, (b) Pd@rGO/ITO, (c) anti-PSA/Pd@rGO/ITO, (d) BSA-anti-PSA/Pd@rGO/ITO. (ii) Electrochemical impedance spectroscopy (EIS) spectra of (a) GO/ITO, (b) rGO/ITO and (c) Pd@rGO/ITO.

broad peak at 23° is an indication of the (002) plane of reduced graphene oxide.

FTIR studies

Fig. 2ii shows the FTIR spectra of GO and Pd@rGO. The spectrum of GO exhibits a band at 1620 cm^{-1} that may be assigned to C=C skeletal vibrations, the bands at 1748 cm^{-1} and 1399 cm^{-1} are due to the stretching vibration of the C=O and C–O bonds present in the carboxylic groups. The band at 1245 cm^{-1} is due to epoxide (C–O–C) groups, the bands at 3420 cm^{-1}, 790 cm^{-1} and 1070 cm^{-1} are due to the OH functional groups. In Pd@rGO, the intensity of these functional groups bands is reduced indicating the mild reduction of GO into rGO. The XRD along with the FTIR data suggest the removal of functional groups between the planes of GO and the incomplete conversion of GO into rGO during the *in situ* synthesis of Pd@rGO.

Structural investigations

Fig. 3i shows the typical scanning electron microscopy (SEM) image of Pd@rGO. Fairly monodispersed Pd nanoparticles can be seen on the surface of rGO which proves their strong affinity for rGO. Fig. 3ii shows the TEM micrograph which supports well the observations made through the SEM investigations. The

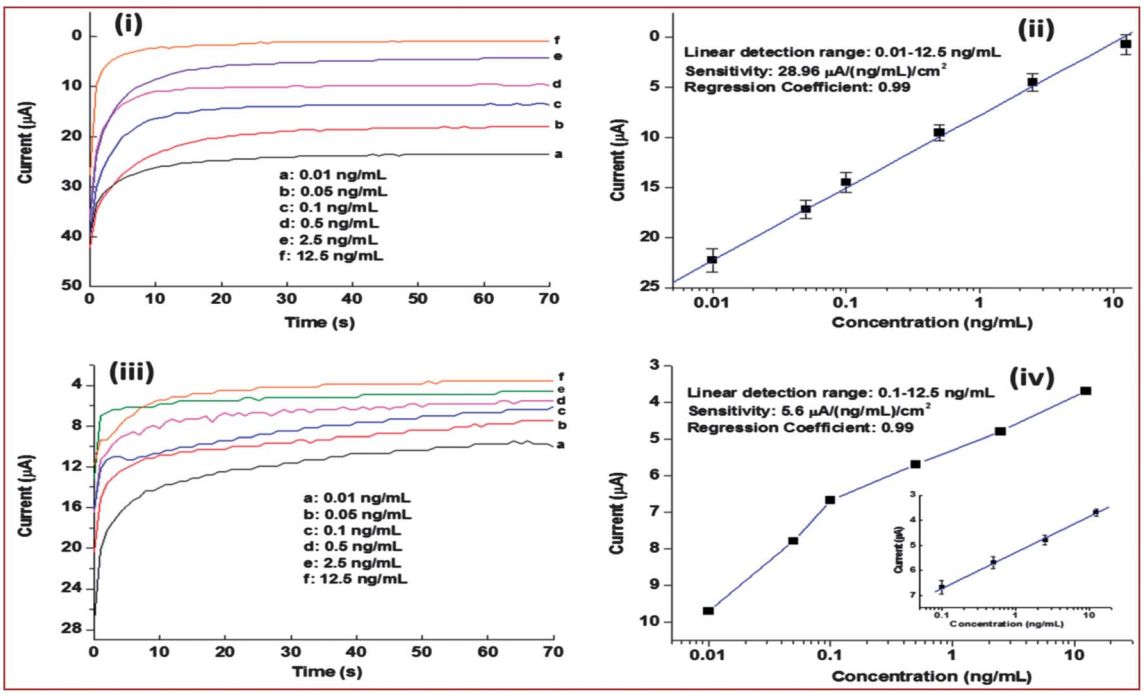

Fig. 5 (i) Chronoamperometric response (at 0.3 V *vs.* Ag/AgCl) studies of the BSA-anti-PSA/Pd@rGO/ITO immunoelectrode as a function of the PSA concentration (0.01–12.5 ng ml^{-1}). (ii) Calibration plot between the current and the PSA concentration for the BSA-anti-PSA/Pd@rGO/ITO immunoelectrode. (iii) Chronoamperometric response of the BSA-anti-PSA/rGO/ITO immunoelectrode as a function of the PSA concentration (0.01–12.5 ng ml^{-1}). (iv) Calibration plot between the current and the PSA concentration for the BSA-anti-PSA/rGO/ITO immunoelectrode, inset: calibration plot obtained for BSA-anti-PSA/rGO/ITO in the linear detection range (0.1–12.5 ng ml^{-1}).

Table 1 Detection of PSA in serum samples

Sample no.	1	2	3	4	5
Amount of PSA in the serum (ng ml^{-1})	0.20	0.20	0.20	0.20	0.20
Amount of PSA added to the serum (ng ml^{-1})	1	2	3	4	5
Amount of PSA recorded by the immunosensor (ng ml^{-1})[a]	1.08	1.96	3.33	4.50	6.05
Recovery(%)[a]	108.0	98.0	111.0	115.0	121.0

[a] Mean of five determinations.

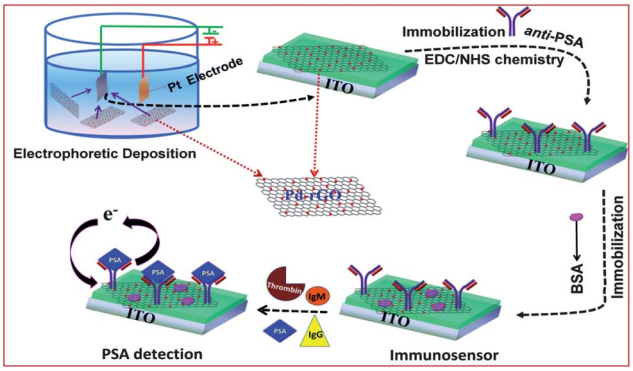

Fig. 6 Schematic representation of the proposed biosensor.

energy dispersive X-ray spectroscopy (EDS) measurements confirm the presence of Pd nanoparticles in the Pd@rGO nanostructure as shown in Fig. 3iii. The size of the Pd nanoparticles ranges from 5 nm to 10 nm, with an average size of around 7 nm as shown in Fig. 3iv (standard deviation, $\sigma = 14.47$).

Electrochemical characterization

Fig. 4i shows the electrochemical cyclic voltammograms (CV) of the (a) rGO/ITO, (b) Pd@rGO/ITO, (c) anti-PSA/Pd@rGO/ITO and (d) BSA-anti-PSA/Pd@rGO/ITO electrodes obtained using an Autolab potentiostat/galvanostat (Eco Chemie, The Netherlands) with a three-electrode system in phosphate buffer saline (PBS, 50 mM, pH 7.0, 0.9% NaCl) containing 5 mM [{Fe(CN)$_6$}$^{3-/4-}$]. The [{Fe(CN)$_6$}$^{3-/4-}$] complex is widely used as a redox probe in electrochemical biosensors as it exhibits well defined redox properties and cyclic voltammograms.[30] It helps for a facile electron transfer at low potentials and thus reduces the possibility of the oxidation of other species or biomolecules that may be present during the detection. Therefore, interference of unwanted species can be avoided. Platinum foil (1 × 1 cm^2) was used as the counter electrode, Pd@rGO/ITO as the working electrode and Ag/AgCl as the reference electrode. The anodic peak current obtained for rGO/ITO at 3.98×10^{-4} A was found to increase to 8.5×10^{-4} A for the Pd@rGO/ITO electrode. The pronounced increment in the current value may be attributed to the excellent electrocatalytic properties resulting from the metallic conductivity of the Pd nanoparticles and the synergistic effects between the Pd nanoparticles and the rGO, which result in a facile electron transfer. After the addition of anti-PSA, the anodic peak current of the anti-PSA/Pd@rGO/ITO electrode decreases to 8.01×10^{-4} A compared to that of Pd@rGO/ITO (8.5×10^{-4} A) due to the insulating nature of the antibodies. The current is further reduced to 5.2×10^{-4} A after the incorporation of BSA due to the macromolecular structure of BSA that block most of the non-specific active sites present on the surface of the anti-PSA/Pd@rGO/ITO immunoelectrode. The surface concentration (I_p) of the BSA-anti-PSA/Pd@rGO/ITO immunoelectrode was calculated using the Brown–Anston model (eqn (1)).

$$I_p = n^2F^2\ I^*\ AV/4RT \quad (1)$$

Where, n is number of electrons transferred, F is Faraday constant (96 485.5 C mol^{-1}), I^* is surface concentration (mol cm^{-2}), A is surface area of the electrode (0.5 cm^2), V is the scan rate (50 mV s^{-1}), R is gas constant (8.134 mol^{-1} K) and T is the room temperature (298 K). The surface concentration of the BSA-anti-PSA/Pd@rGO/ITO immunoelectrode was found to be 3.92×10^{-8} mol cm^{-2}. Moreover, electrochemical impedance spectroscopy (EIS) studies were carried out to investigate the enhanced electrochemical activity of the Pd@rGO nanocomposite (Fig. 4ii). The EIS spectra for the electrodes: (a) GO/ITO, (b) rGO/ITO and (c) Pd@rGO/ITO were obtained using an Autolab potentiostat/galvanostat (Eco Chemie, Netherlands) with a three-electrode system in PBS containing 5 mM [{Fe(CN)$_6$}$^{3-/4-}$]. The charge transfer resistance (R_{ct}) was obtained from the diameter of the semicircle. The R_{ct} values for the GO/ITO, rGO/ITO and rGO@Pd/ITO electrodes were found to be 1.79, 1.32 and 1.15 kΩ respectively, which indicate the enhanced conductivity of the Pd@rGO/ITO nanocomposite electrode compared to both the rGO/ITO electrode as well as the GO/ITO electrode.

Electrochemical response studies

Electrochemical response studies of the BSA-anti-PSA/Pd@rGO/ITO immunoelectrode have been investigated as a function of the antigen (PSA) concentration (0.01–12.5 ng ml^{-1}) using the chronoamperometric method (at 0.3 V *vs.* Ag/AgCl) (Fig. 5i). It has been observed that the anodic peak current decreases as a function of the PSA concentration. It may be related to the very large 2-D surface area of the nanostructure which provides a suitable microenvironment for the strong covalent functionalization of anti-PSA on the Pd@rGO electrode surface. The

reduction in response current may be related to the formation of insulating immunocomplex between Anti-PSA and PSA that hinders electron transport. Fig. 5ii shows the calibration plot obtained between the current and the PSA concentration. The value of current varies linearly with the logarithm of the PSA concentrations and obeys eqn (2).

$$I_p = -7.8 \times 10^{-6}\,(\mathrm{A}) + 7.24 \times 10^{-6}\,(\mathrm{A})\ \log[\text{concentration (ng ml}^{-1})] \quad (2)$$

Regression coefficient (R^2) = 0.992;

The Pd@rGO based immunosensor shows a high sensitivity of 28.96 μA ml ng^{-1} cm^{-2} in the linear detection range of 0.01–12.5 ng ml^{-1}. Further, it can detect PSA at concentrations as low as 10 pg ml^{-1}. The sensing performance of the Pd@rGO/ITO based electrode was compared to the rGO/ITO electrode towards PSA sensing [Fig. 5iii and iv]. The BSA-anti-PSA/rGO/ITO electrode shows a sensitivity of 5.6 μA ml ng^{-1} cm^{-2} and it can detect PSA at concentrations as low as 100 pg ml. The Pd@rGO/ITO based immunosensor exhibits a higher sensitivity than the one based on rGO/ITO which is attributed to its synergistically improved conductivity and larger surface area. Further, the Pd@rGO/ITO based immunosensor displays a wider linear detection range (0.01–12.5 ng ml^{-1}) compared to that of the one based on rGO/ITO (0.1–12.5 ng ml^{-1}). We have compared the sensing characteristics of rGO and Pd@rGO based immunoelectrodes in Table S1 in the ESI† which indicates that the Pd@rGO/ITO based electrode shows a superior sensing performance compared to the rGO/ITO electrode towards PSA detection.

The reproducibility (Fig. S1, see the ESI†) of the proposed immunosensor was investigated by measuring the CV current response of 5 different BSA-anti-PSA/Pd@rGO/ITO immunoelectrodes prepared under the same conditions, in the presence of 1 ng ml^{-1} of PSA. An average current of 600 μA with a relative standard deviation (RSD) of 3% was recorded, which indicates an excellent reproducibility.

The specificity (Fig. S2, see ESI sheet†) of the developed immunosenor was examined by taking the CV response current of the immunolectrode in the presence of other interfering molecules that are commonly found in serum such as IgG, IgM, thrombin or lysozyme along with PSA at a 30 fold concentration. No significant change in the current response was appreciated by the presence of these interfering species which shows the high specificity of the BSA-anti-PSA/Pd@rGO/ITO immunoelectrode for PSA.

In order to evaluate the feasibility of the proposed immunosenor for the analysis of real biological samples, various concentrations of PSA were added to normal serum samples and detection was carried out with the immunosensor. Table 1 shows that the recovery of the PSA added to the serum ranged from 99.8% to 112%, which is in acceptable range.

Further, the stability (Fig. S3, see the ESI†) of the developed immunosensor was evaluated by storing it for 48 days in ambient conditions. The stability of the immunosensor was determined by measuring the CV response of the BSA-anti-PSA/Pd@rGO/ITO immunoelectrode containing 1 ng ml^{-1} of the PSA biomarker at regular intervals of 1 week. Only a 5% decrease in the response current was noticed within 48 days, which indicates its good stability. The sensing characteristics of the proposed BSA-anti-PSA/Pd@rGO/ITO immunosensor along with some of those reported in the literature have been summarized in Table S1 (see the ESI†). The fabrication of the BSA-anti-PSA/Pd@rGO/ITO based immunosensor for cancer detection has been illustrated with the schematic diagram shown in Fig. 6.

Conclusions

We demonstrate a facile single step method for the synthesis of Pd@rGO with an improved conductivity and the preservation of enough functional groups. Further, this nanostructured material has been employed in the development of a label free electrochemical immunosensor for ultrasensitive detection of prostate-specific antigen, a prostate cancer biomarker. The synthesis of Pd@rGO has been confirmed by XRD, FTIR, SEM and TEM micrographs. Pd@rGO has been electrophoretically deposited on an ITO coated glass electrode which was later functionalized with anti-PSA antibodies. The electrochemical sensing results of the proposed immunosensor indicate a high sensitivity of 28.96 μA ml ng^{-1} cm^{-2} in the linear detection range of 0.01–12.5 ng ml^{-1}. The enhanced sensitivity and improved detection range are attributed to the synergistically improved conductivity and the large surface area with enough functional groups in the Pd@rGO nanostructure, which result in high loadings of anti-PSA and enable large scale redox conversions. The proposed immunosensor can be further explored as a reliable point of care diagnostic tool for the detection of other cancer biomarkers.

Acknowledgements

V. K. acknowledges UGC, New Delhi, India, for providing financial support as RGNF. P. S. Saxena acknowledges the CAS program in the Zoology Department, B.H.U., Varanasi, India, funded by UGC. A. Srivastava acknowledges the DST, New Delhi, India, and CAS Department of Physics, Banaras Hindu University, India. S. S. thanks the CSIR, New Delhi, India for providing senior research fellowship (SRF: 31/001(0302)/2008-EMRI).

References

1 S. H. Landis, T. Murray, S. Bolden and P. A. Wingo, *Ca-Cancer J. Clin.*, 1999, **49**, 8–31.
2 C. Fernández-Sánchez, C. J. McNeil, K. Rawson and O. Nilsson, *Anal. Chem.*, 2004, **76**, 5649–5656.
3 C. Fernández-Sánchez, A. M. Gallardo-Soto, K. Rawson, O. Nilsson and C. J. McNeil, *Electrochem. Commun.*, 2004, **6**, 138–143.
4 S. R. Denmeade, I. Litvinov, L. J. Sokoll, H. Lilja and J. T. Isaacs, *Prostate*, 2003, **56**, 45–53.
5 S. P. Balk, Y.-J. Ko and G. J. Bubley, *J. Clin. Oncol.*, 2003, **21**, 383–391.

6 F. Yu, B. Persson, S. Löfås and W. Knoll, *Anal. Chem.*, 2004, **76**, 6765–6770.
7 Y. Seto, T. Iba and K. Abe, *J. Biolumin. Chemilumin.*, 2001, **16**, 285–290.
8 Z. Ye, M. Tan, G. Wang and J. Yuan, *Anal. Chem.*, 2004, **76**, 513–518.
9 T. Soukka, J. Paukkunen, H. Härmä, S. Lönnberg, H. Lindroos and T. Lövgren, *Clin. Chem.*, 2001, **47**, 1269–1278.
10 T. R. G. K. L. Moore, A. F. Dalley, A. M. R. Agur and P. W. Tank, *Clinically Oriented Anatomy*, Lippincott Williams & Wilkins, Baltimore, 1999, vol. 5.
11 X. Tang, S. Bansaruntip, N. Nakayama, E. Yenilmez, Y.-L. Chang and Q. Wang, *Nano Lett.*, 2006, **6**, 1632–1636.
12 T. Yasukawa, Y. Hirano, N. Motochi, H. Shiku and T. Matsue, *Biosens. Bioelectron.*, 2007, **22**, 3099–3104.
13 B. Lim, M. Jiang, P. H. C. Camargo, E. C. Cho, J. Tao, X. Lu, Y. Zhu and Y. Xia, *Science*, 2009, **324**, 1302–1305.
14 X. Q. Zeng, M. L. Latimer, Z. L. Xiao, S. Panuganti, U. Welp, W. K. Kwok and T. Xu, *Nano Lett.*, 2011, **11**, 262–268.
15 J. Watt, S. Cheong, M. F. Toney, B. Ingham, J. Cookson, P. T. Bishop and R. D. Tilley, *ACS Nano*, 2010, **4**, 396–402.
16 O. M. Wilson, R. W. J. Scott, J. C. Garcia-Martinez and R. M. Crooks, *J. Am. Chem. Soc.*, 2005, **127**, 1015–1024.
17 X. Chen, G. Wu, J. Chen, X. Chen, Z. Xie and X. Wang, *J. Am. Chem. Soc.*, 2011, **133**, 3693–3695.
18 M.-P. Pileni, *Nat. Mater.*, 2003, **2**, 145–150.
19 Y. Li, X. Fan, J. Qi, J. Ji, S. Wang, G. Zhang and F. Zhang, *Nano Res.*, 2010, **3**, 429–437.
20 B. M. Choudary, S. Madhi, N. S. Chowdari, M. L. Kantam and B. Sreedhar, *J. Am. Chem. Soc.*, 2002, **124**, 14127–14136.
21 Z. H. Zhang and Z. Y. J. Wang, *J. Org. Chem.*, 2006, **71**, 7485–7487.
22 A. Mastalir, Z. Kiral, M. Benko and I. Dekany, *Catal. Lett.*, 2008, **124**, 34–38.
23 A. Mastalir, Z. Kiraly, A. Patzko, I. Dekany and P. L. Argentiere, *Carbon*, 2008, **46**, 1631.
24 Y. Li, X. Fan, J. Qi, J. Ji, S. Wang, G. Zhang and F. Zhang, *Nano Res.*, 2010, **3**, 429–437.
25 G. M. Scheuermann, L. Rumi, P. Steurer, W. Bannwarth and R. Mulhaupt, *J. Am. Chem. Soc.*, 2009, **131**, 8262–8270.
26 P. A. Khomyakov, G. Giovannetti, P. C. Rusu, G. Brocks, J. van den Brink and P. J. Kelly, *Phys. Rev. B*, 2009, **79**, 195425–195436.
27 G. Lu, S. Mao, S. Park, R. S. Ruoff and J. Chen, *Nano Res.*, 2009, **2**, 192–200.
28 H. Li, L. Han, J. J. Cooper-White and I. Kim, *Nanoscale*, 2012, **4**, 1355–1361.
29 D. C. Marcano, D. V. Kosynkin, J. M. Berlin, A. Sinitskii, Z. Sun, A. Slesarev, L. B. Alemany, W. Lu and J. M. Tour, *ACS Nano*, 2010, **4**, 4806–4814.
30 S. Srivastava, V. Kumar, A. Ali, P. R. Solanki, A. Srivastava, G. Sumana, P. S. Saxena, A. G. Joshi and B. D. Malhotra, *Nanoscale*, 2013, **5**, 3043–3051.